diffusion-fundamentals.org
The Open-Access Journal for the Basic Principles of Diffusion Theory, Experiment and Application

Axon radius estimation with Oscillating Gradient Spin Echo (OGSE) Diffusion MRI

Bernard Siow[1,2], Ivana Drobnjak[1], Andrada Ianus[1], Isabel N. Christie[2], Mark F. Lythgoe[2] and Daniel C. Alexander[1]

[1] Centre for Medical Image Computing, University College London, UK
[2] Centre for Advanced Biomedical Imaging, University College London, UK

Corresponding author: Bernard Siow, Center for Medical Image Computing, Malet Place, University College London, UK. E-Mail: b.siow@ucl.ac.uk

Abstract

The estimation of axon radius provides insights into brain function [1] and could provide progression and classification biomarkers for a number of white matter diseases [2-4]. A recent in silico study [5] has shown that optimised gradient waveforms (GEN) and oscillating gradient waveform spin echo (OGSE) have increased sensitivity to small axon radius compared to pulsed gradient spin echo (PGSE) diffusion MR sequences. In a follow-up study [6], experiments with glass capillaries show the practical feasibility of GEN sequences and verify improved pore-size estimates. Here, we compare PGSE with sine, sine with arbitrary phase, and square wave OGSE (SNOGSE, SPOGSE, SWOGSE, respectively) for axon radius mapping in the corpus callosum of a rat, ex-vivo. Our results suggest improvements in pore size estimates from OGSE over PGSE, with greatest improvement from SWOGSE, supporting theoretical results from [5] and other studies [7-9].

Keywords

Axon diameter, diffusion MR, oscillating gradient spin echo, optimised gradient waveform, ActiveAx.

1. Introduction

Diffusion MRI is used clinically to elucidate biological tissue microstructure [10]. To date, the vast majority of these investigations quantify measures that assume Gaussian diffusion, such as mean diffusivity (MD) or fractional anisotropy (FA). Recently, there has been increasing interest in fitting biophysical models of tissue to measured signals [11-14]. These model-based approaches can directly estimate tissue parameters such as cell size, density, intra- and extra-cellular diffusivities. Of particular interest here is the ActiveAx technique [14] that uses a simplified model of white matter that can represent tissue sufficiently well, and in which there is no prior knowledge of orientation. This simplified model reduces the number of model parameters and, coupled with optimisation of the protocol, reduces the total

number of measurements needed. This potentially allows the use of the ActiveAx technique in clinical scenarios in which total scan time is an important factor.

Conventionally, the trapezoid gradient waveforms in the PGSE sequence are used to sensitise the MR signal to diffusion. Reliable estimates of small axon radii (<5 μm) require high gradient amplitudes and short diffusion times, which limits the suitability of PGSE sequences for microstructure estimates in a clinical setting. OGSE sequences have shorter diffusion times and thus can probe shorter length scales [5, 15-19]. A recent in silico study [5], which optimises the shape of the gradient waveform (GEN, see Figure 1), suggests that the optimal gradient waveform for pore-size estimation, particularly for small radii, consists of oscillating trapezoids. We followed up this study by implementing GEN protocols on a 9.4T small bore scanner using glass microcapillaries with a range of radii (1-10 μm) and gradient amplitudes (0.04-0.2 T/m) [6]. We found an excellent agreement between simulated and measured signal (Figure 2) and verified that GEN has greater sensitivity to small pore radii compared to PGSE, particularly at the low gradient strengths achievable by clinical scanners. We see this in the posterior distribution on pore radius for a maximum gradient

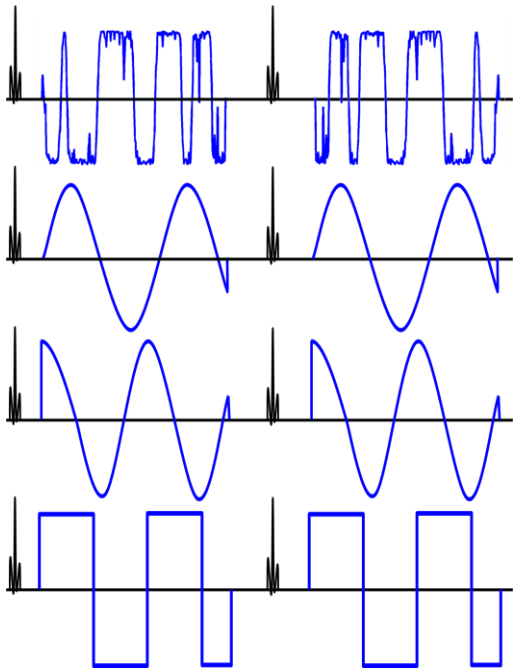

Figure 1. Schematic of GEN, SNOGSE, SPOGSE and SWOGSE sequences (top to bottom)

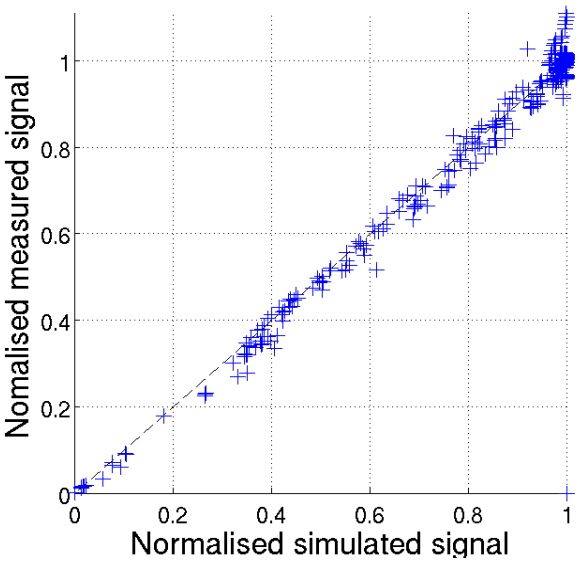

Figure 2. Measured vs simulated signal for GEN sequences

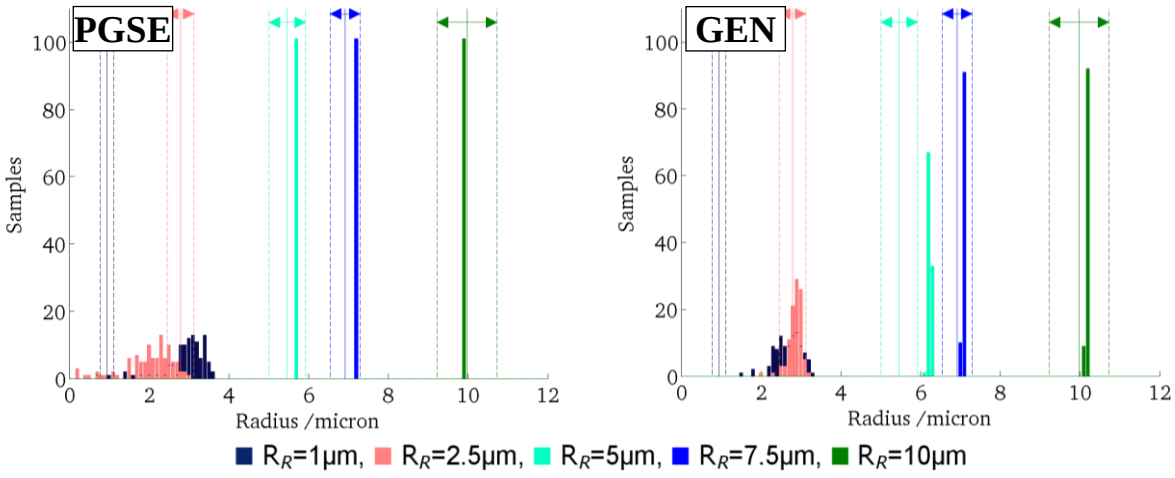

Figure 3. Histograms of posterior distribution on pore radius for microcapillaries, for maximum gradient strength = 40mT/m. Solid lines and dotted lines represent pore radius index measured by scanning electron microscopy.*

strength of 0.04T/m (Figure 3): capillaries with radius R_R=1µm (blue) and R_R=2.5µm have posterior distributions that are narrower for GEN than for PGSE. Furthermore, the modes of these distributions are closer to the radius measured by electron microscopy for GEN than for PGSE. For both protocols we lose sensitivity at lower pore radii, but the lowest distinguishable radius is lower for GEN than PGSE. The overestimation by GEN of R_R=1µm may also arise from surface imperfections in the sample [6].

The signal model used in [5] is computed numerically using the matrix method [16,5], which is computationally expensive. This makes mapping axon radius across the corpus callosum using GEN waveforms impractical. The analytical Gaussian Phase Distribution (GPD) approximation signal model is orders of magnitude faster and agrees with Monte Carlo simulations well [20]. GPD has been used to efficiently calculate signal for sine, sine with arbitrary phase and square wave OGSE (SNOGSE, SPOGSE, SWOGSE respectively) [20].

In this study, we map axon radius across the corpus callosum of an ex-vivo rat brain, without prior knowledge of axon orientation. We compare PGSE, SNOGSE, SPOGSE, and SWOGSE ActiveAx protocols. We use GPD signal model for optimisation and voxel-by-voxel fitting, thus making orientationally invariant axon radius maps using OGSE feasible and practical.

2. Methods

2.1. Optimisation

We adapted the optimization framework as described in [5,14,21]. The tissue model consisted of impermeable parallel cylinders with impermeable walls and an extra-axonal compartment, as described in [14,5]. For this study, we optimised the length, duration, frequency and phase of the waveforms for a fixed gradient magnitude of 400 mTm^{-1}. The protocols were optimised for sensitivity to fibre radii of 0.5, 1, 2.5 & 5µm. The number of measurements per protocol was 6 in 60 directions (360 scans per protocol) plus 12 scans without diffusion weighting for normalization.

2.2. MRI

The optimised protocols were implemented on a 9.4T Agilent Technologies, Inc. pre-clinical system equipped with gradient capable of $1Tm^{-1}$ with a rise time of 200µs. A 26mm diameter Rapid Biomedical, GmBH r.f. coil was used. A 4-shot (k-space segmented) EPI readout was used with the following imaging parameters: TR = 3s, TE = 60ms, 1 x 1mm slice, 128x128 matrix, 12x24mm FoV. Total scan time per protocol was 2.55 hours.

2.3. Sample

A Sprague Dawley rat was perfuse fixed using 4% formaldehyde solution from paraformaldehyde (PFA). The brain was extracted and stored in 4% PFA for 2 weeks. The sample was then immersed in phosphate buffer solution for >1week. Prior to imaging, the sample was placed in a plastic cylindrical container filled with Fomblin Perflourosolv™ PFS-1 (Solvay Solexis, Inc.), which is not visible in proton MR. The sample temperature was maintained at 18.5±0.5°C during the scans.

2.4. Fitting

A three stage fitting procedure detailed in [21] was used. Briefly this consisted of a grid search, gradient descent, and Markov Chain Monte Carlo (MCMC) procedures. An ex-vivo white matter tissue model described in [21] (zeppelin-cylinder-dot in the taxonomy in [22]) was used. Briefly, the model consisted of parallel cylinders of single radius, an extra axonal compartment, an isotropic CSF compartment, and a stationary trapped water compartment,

with no exchange between the compartments. For the grid search and gradient descent all model parameters were fitted except diffusivity of the CSF compartment and free diffusivity inside and outside the cylinders (set to 2 and 0.6 $x10^{-9}$ m^2s^{-1}, respectively). For the MCMC only volume fraction and radius were fitted. The MCMC fitting ran 200000 iterations, with a burn-in of 10000 iterations, which were discarded. We took every 200^{th} sample from the MCMC run to get 1000 estimates of the model parameters. Thus, we estimated the single axon radius in this tissue model 1000 times. We call the mean of these estimates the axon radius index. The axon radius index should correlate with the mean axon radius weighted by axon volume within the pixel [21].

3. Results

3.1. Optimisation

The optimised protocols can be found in Figure 4. All protocols have a mix of long (separated single mode pulses) and short diffusion times (high frequency oscillations in OGSE protocols) and OGSE protocols have a wider range of diffusion times. At low oscillation frequencies, SPOGSE sequences can approximate PGSE, whereas SNOGSE sequences cannot. Thus SNOGSE sequences have low attenuation at long diffusion times. Of note, we find that SPOGSE waveforms mostly have phase of $\pi/2$ (or - $\pi/2$). This is consistent with studies that consider the gradient power modulation spectrum, which use cosine waveforms [15-17]. We also note that the optimisation finds very similar combinations of measurements within each protocol.

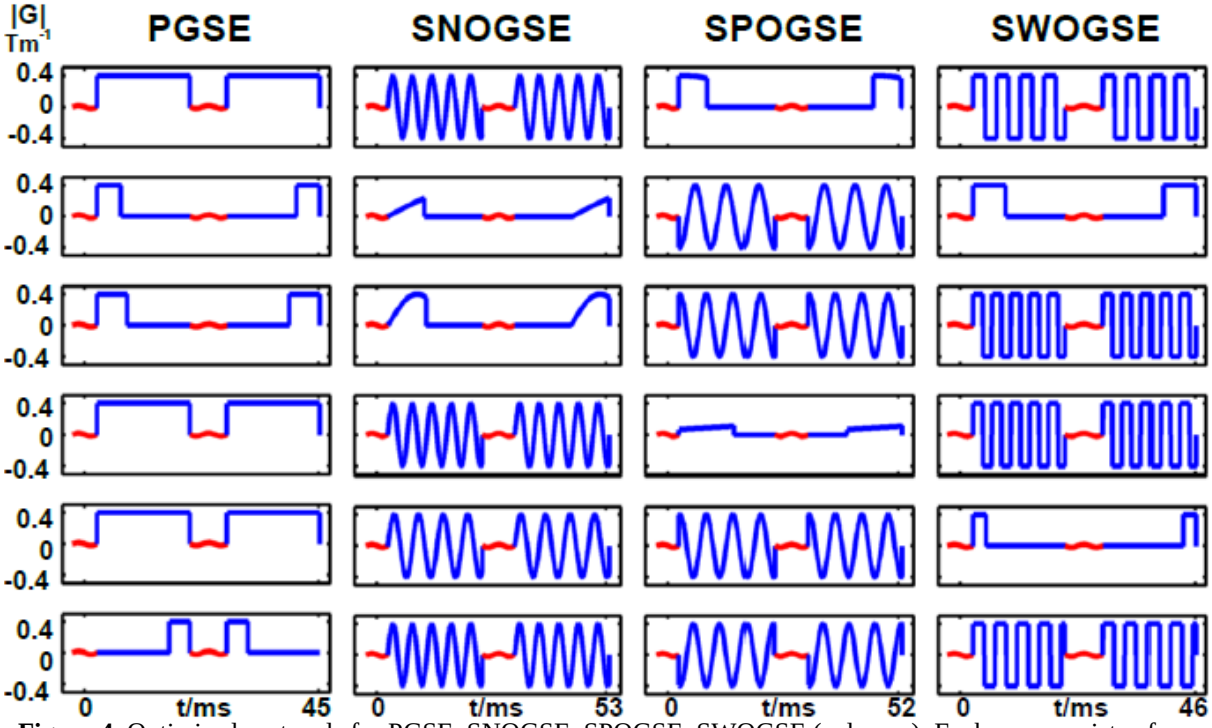

Figure 4. Optimised protocols for PGSE, SNOGSE, SPOGSE, SWOGSE (columns). Each row consists of one of the six measurements.

3.2. Axon radius index estimates

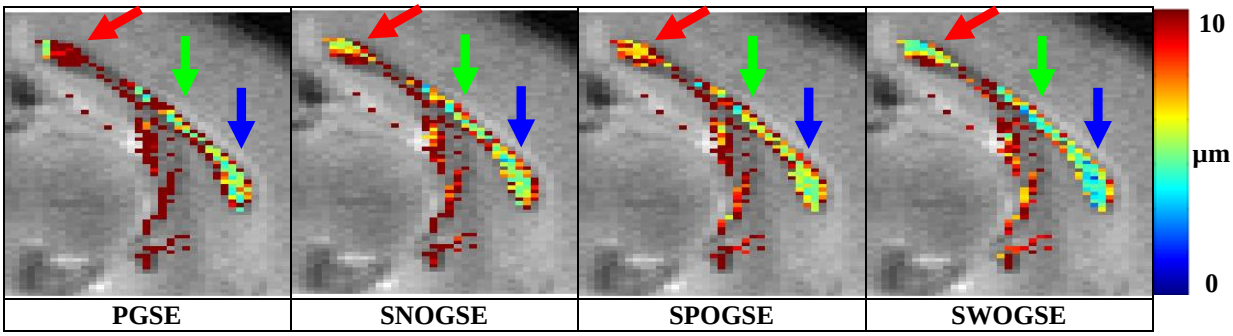

Figure 5. Axon radius index maps overlaid on images without diffusion weighting. Red, green and blue arrows point to splenium, midbody, and genu, respectively

Figure 5 shows maps of axon radius index over the mid-sagittal corpus callosum (pixels with linearity [23] < 0.3 were excluded from the maps). We see that the axon radius index is consistently lower in OGSE compared to PGSE protocols, and lowest with SWOGSE. We expect greater sensitivity to small radii from SWOGSE because it packs more diffusion weighting into each period of the oscillation. Thus SWOGSE has the ability to have greater attenuation at shorter length scales, which increases sensitivity to smaller pores. In the splenium, estimates of axon radius index for PGSE protocols are higher compared to OGSE protocols. From histological studies [24,25], we expect the variation along the corpus callosum to be smaller than the estimates from the PGSE protocol.

Figure 6 shows the distribution of the estimates of axon radius from the 1000 MCMC samples (i.e. the posterior distribution on the axon radius index) for representative pixels in the splenium, midbody, and genu of the corpus callosum. We observe that the posterior distributions are consistent between protocols (overlapping distributions with similar modes) and, in general, narrow from PGSE to SNOGSE to SPOGSE to SWOGSE, suggesting that SWOGSE protocols have better precision in the axon radius index. This trend was also observed for the vast majority of other voxels (data not shown).

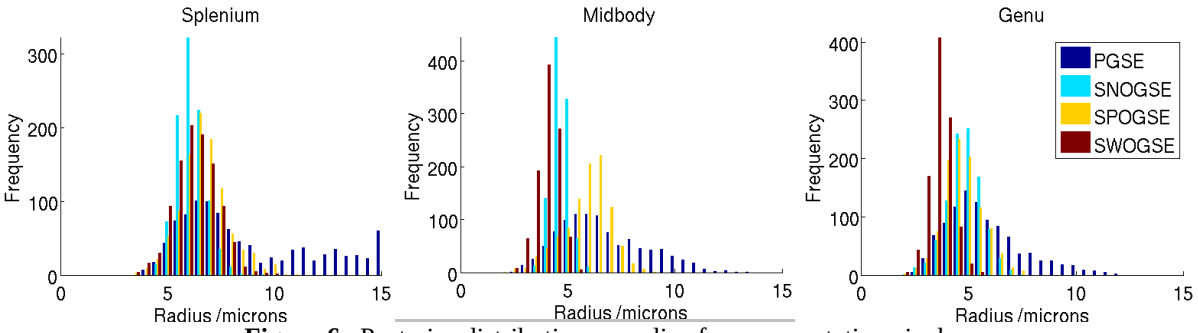

Figure 6. Posterior distribution on radius for representative pixels

4. Conclusions

We have optimised PGSE, SNOGSE, SPOGSE, and SWOSGE protocols for ActiveAx allowing orientationally invariant axon radius index mapping, which we demonstrate in the ex-vivo rat corpus callosum. This is the first demonstration of OGSE to estimate axon radius. We find that the posterior distributions on axon radius index are quite consistent across all protocols and that the axon radius index is most precise for SWOGSE. These findings should extend to pore size estimation in general. Future work will extend to in vivo and clinical scenarios: the total number of scans in each of the protocols (360+12) is achievable in those scenarios [21].

5. References

[1] J.M. Ritchie, Proc. R. Soc. B: Biol. Sci. 217 (1206) (1982) 29–35
[2] J. Piven, et al, Am. J. Psych. 154 (8) (1997) 1051–1056.
[3] S. Cluskey, D.B. Ramsden, Mole. Pathol.: MP 54 (6) (2001) 386–392.
[4] P.L. Randall, Med. Hypoth. 10 (3) (1983) 247–280.
[5] I. Drobnjak et al, J Magn Reson 206 (1) (2010) 41-51
[6] B. Siow et al, J Magn Reson 214 (2012) 51-60
[7] M.D. Does, et al, Magn. Reson. Med. 49 (2) (2003) 206–215
[8] J. Xu, Proc Intl Soc Mag Reson Med 20 (2012) 0351
[9] A.T. Van, Proc Intl Soc Mag Reson Med 20 (2012) 0354
[10] P.J. Basser, NMR Biomed. 8 (7) (1995) 333–344,
[11] G.J. Stanisz, st al, Magn. Reson. Med. 37 (1) (1997) 103-111
[12] Y. Assaf,. Magn. Reson. Med. 59 (6) (2008): 1347–1354.
[13] Y. Assaf, P.J. Basser, NeuroImage 27 (1) (2005) 48–58
[14] D.C. Alexander, Magn. Reson. Med. 60 (2) (2008) 439–448
[15] J. Xu, et al, Magn. Reson. Med. 61 (4) (2009) 828-833
[16] P. Callaghan, et al, Adv Magn Opt Reson 19 (1996) 325–388
[17] E. Parsons, et al, Magn Reson Imaging 21 (1) (2003) 279–285
[18] M. Schachter, et al, J Magn Reson 146 (2000) 232–237.
[19] M. Aggarwal, et al, Magn Reson Med. 67 (1) (2012):98-109
[20] A. Ianus, et al, Proc Intl Soc Mag Reson Med 20 (2012) 3561
[21] D.C. Alexander, et al, Neuroimage 52 (4) (2010) 1374-89
[22] E. Panagiotaki, et al, Neuroimage 59 (3) (2012) 2241-54
[23] C.F. Westin, et al, Proc. MICCAI'99, LNCS-1679, (1999) 441–452.
[24] S. Waxman. The Axon : Structure, Function, and Pathophysiology, OUP, 1995
[25] D. Barazany, Brain 132, (5) (2009) 1210–1220

* Reprinted from [6] with permission from Elsevier